ADVANCED FUNCTIONAL MATERIALS
www.afm-journal.de

Biocompatible Electromechanical Actuators Composed of Silk-Conducting Polymer Composites

*Isabella S. Romero, Nathan P. Bradshaw, Jesse D. Larson, Sean Y. Severt, Sandra J. Roberts, Morgan L. Schiller, Janelle M. Leger, and Amanda R. Murphy**

Single-component, metal-free, biocompatible, electromechanical actuator devices are fabricated using a composite material composed of silk fibroin and poly(pyrrole) (PPy). Chemical modification techniques are developed to produce free-standing films with a bilayer-type structure, with unmodified silk on one side and an interpenetrating network (IPN) of silk and PPy on the other. The IPN formed between the silk and PPy prohibits delamination, resulting in a durable and fully biocompatible device. The electrochemical stability of these materials is investigated through cyclic voltammetry, and redox sensitivity to the presence of different anions is noted. Free-end bending actuation performance and force generation within silk-PPy composite films during oxidation and reduction in a biologically relevant environment are investigated in detail. These silk–PPy composites are stable to repeated actuation, and are able to generate forces comparable with natural muscle (>0.1 MPa), making them ideal candidates for interfacing with biological tissues.

1. Introduction

In recent decades, there has been a growing interest in the development of systems capable of biomimetic movements that are not achievable with standard motors. In addition, materials capable of controlled movements that can also interface with biological environments are highly sought after to fill a niche as biomedical devices[1] such as steerable catheters,[2] valves, blood vessel sutures, cochlear implants and controlled drug release devices.[3] Conducting polymers (CPs) possess a variety of attributes that make them particularly well suited for such applications.[1] CPs, such as poly(pyrrole) (PPy), undergo volume changes due to ion/solvent diffusion in and out of the polymer matrix upon electrochemical switching between oxidized and reduced states.[1,4] Depending on whether anion or cation exchange predominates, the active layer will either 1) expand upon oxidation due to anion insertion and contract upon reduction due to anion expulsion or 2) contract on oxidation due to cation expulsion and expand on reduction due to cation insertion. Actuators based on CPs can be electrically controlled at low operating voltages (typically 1–3 V), continuously switched between expanded/contracted states, and operate well in liquid electrolytes. Interfacing CPs with biological systems is also possible due to the demonstrated biocompatibility *in vitro* and *in vivo*.[5,6] To date, record-breaking CP actuators have been demonstrated to generate stresses as large as 100 MPa[7] and strains up to 40%,[8] although the generation of both high stress and high strain has yet to be achieved. Typical CP actuators can generate smaller, yet still notable, stresses of 1–5 MPa with strains on the order of 2%.[9]

These impressive values have led to commercial interest in the development of several types of biomedical devices utilizing CP actuators.[1,9] However, current optimized device designs are not ideal for applications requiring implantation *in vivo*. Major difficulties encountered when fabricating CP-based actuators arise from the fact that the bulk polymers are brittle and insoluble due to the extended conjugated backbone, which restricts the molding or processing of these materials into 3D structures. Therefore, the majority of CP-based actuators are synthesized via electropolymerization directly onto metal foils,[1] where the metal is often retained in the final device. While metal incorporation helps minimize the iR drop across CP films, these devices are typically limited to 2D film architectures and have significant problems with delamination.[10,11] While useful for surgical and external biomedical applications, incorporation of non-degradable or rigid components[1,12] that are incompatible with soft tissues severely limit the possible applications of CP actuators. In addition, device performance in a biologically-relevant environment is still unclear as the majority of studies utilize optimized electrolyte systems that employ toxic salts or organic solvents.

To avoid the use of metals or rigid inorganic components in the final device, all-polymeric actuators have been constructed by depositing CPs in situ during chemical polymerization onto several types of synthetic backing materials such as PVDF,[13–15] crosslinked PEO-based copolymers,[16–20] and polyurethane.[21] Electropolymerized films have also been transferred from

I. S. Romero, N. P. Bradshaw, J. D. Larson, S. Y. Severt, M. L. Schiller, Prof. A. R. Murphy
Department of Chemistry
Western Washington University
516 High St. Bellingham, WA 98225–9150, USA
E-mail: amanda.murphy@wwu.edu
S. J. Roberts, Prof. J. M. Leger
Department of Physics and Astronomy
Western Washington University
Bellingham, WA 98225–9164, USA

DOI: 10.1002/adfm.201303292

metal electrodes to scotch tape to form bilayer and trilayer devices.[22,23] However, very few reports have been made on construction of composite actuators with biocompatible and biodegradable polymers. Among the limited examples are chitosan composites with poly(aniline) that only operate at very acidic pH,[24,25] and chitosan fibers coated with PPy.[26]

A biopolymer that has yet to be employed in CP composite actuators is silk fibroin, the polypeptide isolated directly from *Bombyx mori* silkworm cocoons. Silk is an attractive support material due to its excellent mechanical properties, biocompatibility, slow degradation profile and aqueous processibility.[27,28] Silk fibers can be dissolved and re-processed into a variety of architectures including 2D films and fibers, or 3D sponges and hydrogels,[27,28] allowing for facile construction of 3D actuator devices. We have previously demonstrated that a diazonium coupling reaction can be used to covalently attach sulfonic acid groups to the tyrosine residues in the silk protein.[29,30] We have also demonstrated that pyrrole can be selectively absorbed and subsequently polymerized within these 'acid-modified' silk films, forming a conductive interpenetrating network (IPN) of PPy and silk.[30] The ability to form this ideal IPN structure inspired us to adapt these materials for use as CP actuators, as one of the main modes of failure for these devices is delamination. In our materials, PPy is completely integrated with the silk film making delamination impossible, resulting in a durable and fully-biocompatible device structure. Here, we detail the fabrication, electrochemical characterization and actuation performance of bilayer bending actuators made from these silk-PPy IPNs.

2. Fabrication of Bilayer Actuator Films

To demonstrate the ability of silk-PPy composites to undergo electromechanical actuation, methods were developed to construct a bilayer device with the active conducting polymer only on one face, and the inactive silk support on the other (**Figure 1**a). This geometry results in a bending movement due to differential expansion of the PPy face of the bilayer device. In addition, methods to increase the surface area of silk films were investigated, as CP actuators rely on the ability of ions to move in and out of the films for expansion and contraction.[4,31] The surface morphology of a silk film is dictated by the surface on which it is cast, and previous studies have demonstrated that the silk-PPy composite films retain the morphology of the initial silk surface after PPy deposition.[30] Therefore, to impart porosity into the surface of the films, aqueous silk solutions were cast onto a silicone baking mat, resulting in ~50 µm thick silk films that were microporous on one face and smooth on the other.

To deposit PPy only on the porous face, films were adhered to the surface of polystyrene Petri dishes with tape prior to the diazonium coupling and pyrrole polymerization reactions (Figure 1a). To ensure one-sided deposition had occurred, films were carefully peeled from the dish after this reaction sequence, and thin cross-sections of the films were cut and imaged with an optical microscope. As shown in Figure 1b, the yellow color indicative of the azo bond between the diazonium salt of sulfanilic acid and the tyrosine residues in silk was observed to

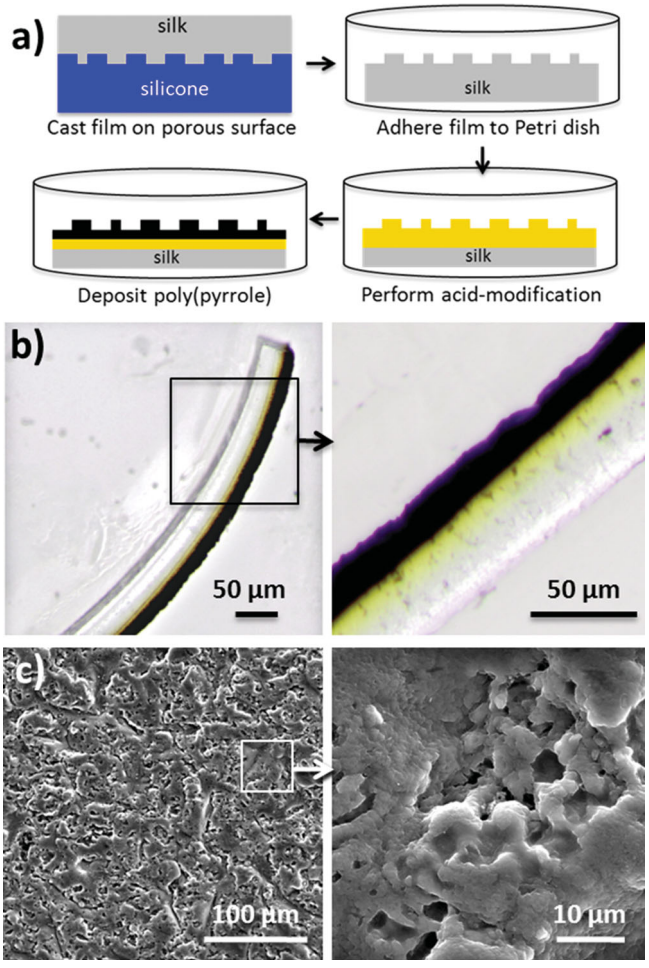

Figure 1. a) Illustration of the bilayer actuator film fabrication process. b) Optical microscope images of thin cross-sections of bilayer actuator films, where the penetration depth of the acid-modification (yellow) and PPy (black) are clearly visible in the transparent silk film. c) SEM images of the porous face of a typical actuator film after acid-modification and PPy deposition (morphology does not change significantly during modification).

penetrate ~25 µm, while the black PPy penetrated ~15 µm into the surface of the films. No color change was observed on the face of the films that were adhered to the dish, indicating that the seal provided by the tape was sufficient to prevent exposure to the chemical reagents. The modified film faces had an average sheet resistivity of ~10^2 Ω/sq, and were conductive enough to be imaged with a scanning electron microscope (SEM) without a metal coating (Figure 1c). Similar to previous studies,[30] the film surfaces were not significantly altered by the reaction sequence, and the films retain the microscale porosity and the nodular morphology seen prior to modification (see Supporting Information).

The addition of small molecule sulfonic acid 'dopants' during the pyrrole polymerization reaction has been shown to dramatically affect the conductivity and stability of the resulting silk-PPy composites.[30] Here we found that the most reproducible actuation was obtained for films where sodium allyl sulfonate (AS) was used. No actuation was observed in silk-PPy films synthesized without an added dopant, and films synthesized

using larger dopants such as *p*-toluene sulfonic acid gave inconsistent actuation behavior, likely due to mixed anion and cation exchange.[32] Because our actuators primarily rely on anion exchange for expansion and contraction (discussed below), retention of larger, less mobile anions in the silk-PPy IPN matrix can hinder the actuation ability.[10,33]

3. Electrochemical Characterization of Actuator Films

Cyclic voltammetry (CV) was employed to evaluate the electrochemical stability of the actuator films, and investigate the effects of electrolyte composition on the electrochemical switching of the PPy. Studies were carried out in a 3-electrode cell equipped with a platinum wire counter electrode and a Ag/AgCl (3 M NaCl) reference electrode. Circular (10–13 mm diameter) silk-PPy films doped with AS served as the working electrodes. While salts such as lithium perchlorate are commonly used as electrolytes for conducting polymer actuators, all of our characterization was completed only in biologically relevant fluids to represent how these materials would perform when implanted *in vivo*.

A representative CV of a film cycled in phosphate buffered saline (PBS, 0.1 M sodium phosphate, 0.15 M NaCl, pH 7.2) is shown in **Figure 2**a. The voltammograms had a broad reduction peak centered at -0.6 V vs. Ag/AgCl, and a broad oxidation peak at +0.5 V. Prolonged cycling in PBS shifted the reduction peak to −0.4 V, but the oxidation stayed fairly consistent (Figure 2a). While the shape of the voltammogram changed, the overall charge storage capacity (area) remained nearly constant from the 10th to the 150th scan. From 150 to 200 scans, films began to slowly degrade as noted by a 30% decrease in the capacitance. While encapsulation within silk films increased the electrochemical stability of the PPy as compared to films deposited on platinum,[34,35] the slow degradation of the PPy under these conditions suggests that these materials will be most appropriate for applications requiring moderate cycling lifetimes.

To further explore how the ion composition of the electrolyte influences the redox processes in the silk-PPy composite films, CV scans were carried out in a range of supporting electrolytes. To investigate the effect of the cation identity, a single film was successively cycled in 0.2 M aqueous solutions of NaCl, KCl, $CaCl_2$, and $MgCl_2$ for five cycles each. A corresponding experiment was carried out using 0.2 M aqueous solutions of NaCl, NaH_2PO_4, $NaHCO_3$, and Na_2CO_3 to examine the role of anion identity. The fourth cycle for each condition is shown in Figure 2b and c. The order that the films were exposed to the electrolytes was randomized for different trials, and did not significantly affect the results.

When cycled in the chloride salts containing different cations, the voltammograms were mostly indistinguishable from one another (Figure 2b). Slight shifts in reduction potential in the presence of monovalent vs. divalent cations were noted, which varied from sample to sample. The magnitude of the shift was smaller, but consistent with previous literature.[36] These voltammograms had the highest capacitance and most ill-defined oxidation and reduction peaks as compared to the other solutions. In contrast to the relative uniformity of the voltammograms in chloride salts, striking differences were noted when films were cycled in the presence of different anions (Figure 2c). The same film cycled in the presence of

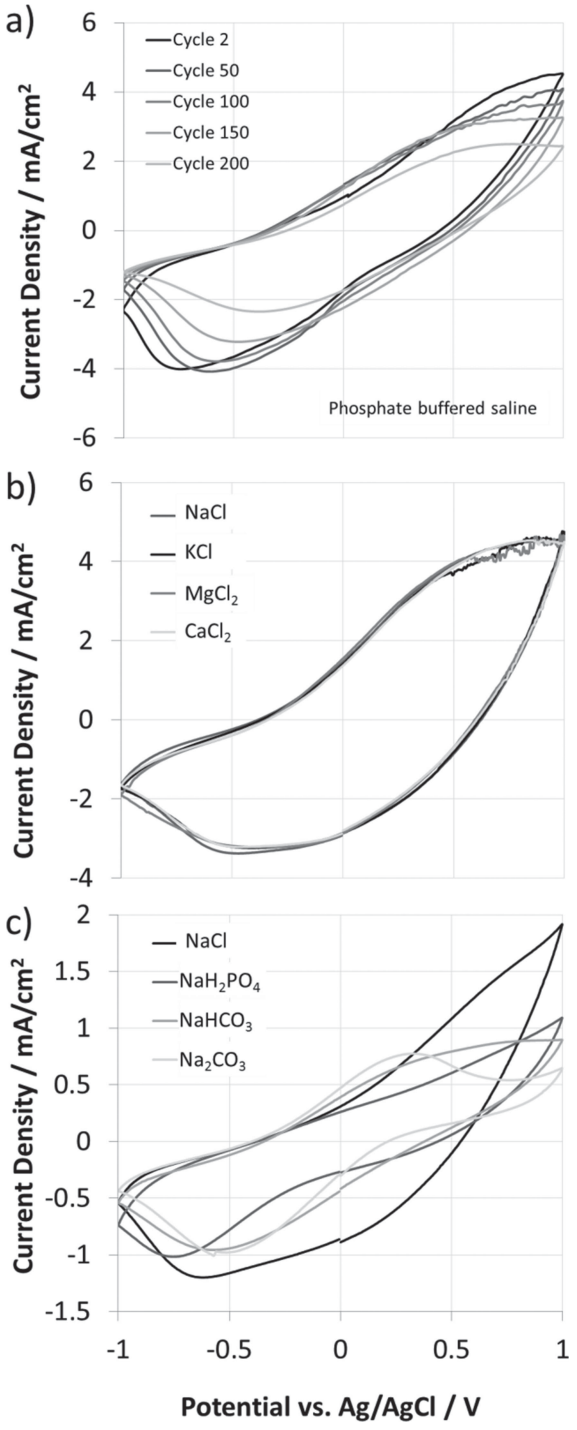

Figure 2. Cyclic voltammograms of silk-PPy composites in biologically-relevant salt solutions. All CVs were performed at a scan rate of 50 mV/s from −1 to +1 V using an Ag/AgCl reference electrode and a platinum wire counter electrode. a) Representative voltammograms of a film cycled extensively in PBS. CVs were also recorded of a single film cycled sequentially in 0.2 M solutions containing b) chloride salts with different cations and c) sodium salts with different anions.

carbonate exhibited lower oxidation and reduction potentials centered around +0.25 V and –0.5 V, respectively, that were particularly pronounced in Na_2CO_3. Capacitance was the lowest when cycled in NaH_2PO_4, and no distinct oxidation peak was observed. The redox characteristics of the individual electrolytes, NaCl and NaH_2PO_4, are both overlaid in the voltammograms in PBS where the two are combined (Figure 2a).

In CPs, the oxidation and reduction of the polymer backbone is inextricably linked to ion/solvent diffusion in and out of the polymer matrix, making CV data difficult to fully interpret.[36–38] However, CV can give some insight into the extent to which different cations and anions participate in the redox processes, which is often tied to the relative ease of ion flow in and out of the PPy matrix.[31,36,39] Here, the consistency seen in the voltammograms obtained in chloride salts with different cations suggests that the presence of the different cationic species do not dramatically influence the redox properties of these silk-PPy composites. However, the identity of the anion does play a role in driving the redox reaction. Here, the monovalent chloride tends to result in over-oxidation of PPy as evidenced by the continued increase in current while sweeping to more positive voltages. Over-oxidation is suppressed when divalent anions are present. This result is consistent with previous studies with PPy that have shown that monovalent, highly mobile anions exhibit a higher propensity for 'over-doping,' which contributes to the large capacitance seen during oxidation.[36,37] This effect is suppressed when only divalent anions are available, which can be attributed to their size, polarity or ineffectual stabilization of charges spread across several pyrrole units.[36]

4. Actuation Performance

4.1. Free-End Bending

The ability of these films to bend under an applied electrical stimulus was demonstrated using a 2-electrode cell, where silk-PPy bilayer films served as the working electrode and platinum mesh was used as the combined reference/counter electrode. Bilayers were positioned with the electroactive side facing the platinum mesh. Electrical contact was made to the films by mechanically fixing the end of the film to a gold foil using an inert plastic clamp. All actuation experiments were carried out in PBS to evaluate performance in a biologically-relevant environment.

Typical experiments began with a 'curing' sequence, where a ±3.0 V square wave was applied for 50 cycles at 1 Hz. While not necessary for actuation, performing this curing sequence resulted in more consistent macroscale actuation behavior. Literature suggests that CP actuators undergo a reorganizational process during the first several oxidation and reduction cycles, where the linear polymer chains restructure as the dopant ions present in the synthesized film equilibrate with the ions in the electrolyte solution.[31,40] Fast cycling rates can minimize the electrochemical degradation of CPs,[41] therefore 1 Hz cycles were chosen for this initial curing sequence. As shown in **Figure 3**, current levels plateau between 10–100 cycles when applying a square wave potential at 1 Hz, so 50 cycles were chosen for the curing cycle. A decay in current

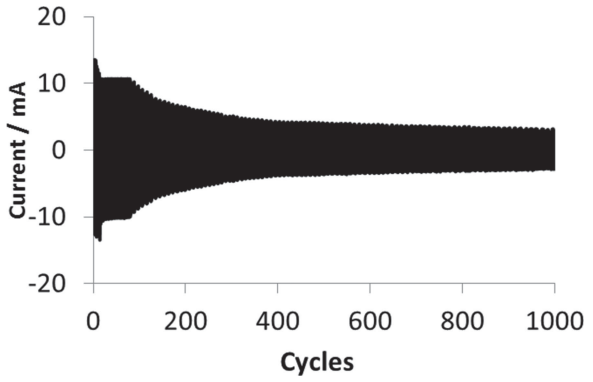

Figure 3. Current response measured over time when a ±3.0 V square wave is applied to a silk-PPy bilayer for 1000 cycles at 1 Hz.

is noted over extended cycling, where a 50% drop in current occurs between cycle 100–250, similar to the trend observed in CV. After 250 cycles the actuator current stabilizes, and only very gradual further decay is noted. While maximal movement is not achieved at this frequency, the films did actuate for all 1000 cycles, resulting in an observable oscillation throughout the entire sequence (see movie in Supporting Information).

For maximal actuation, immediately following the fast curing sequence a ±3.0 V square wave was applied to the films at two-minute intervals. **Figure 4**a–c displays overlaid images representative of the typical bending motions observed, and the angle of deflection throughout 16 full cycles. A plot of the applied voltage and measured current for these cycles is shown in Figure 4d. In all cases, the silk-PPy composites contracted under reduction and expanded under oxidation, suggesting that the bilayer films operate primarily by anion exchange. In this mechanism, counter anions and accompanying solvent molecules are expelled when the cationic PPy is reduced to its neutral form, resulting in a contracting motion. Upon oxidation, the anions are re-inserted, resulting in expansion or stiffening of the film.

During the initial 50-cycle curing sequence, films typically exhibited a net expansion in addition to the observed oscillation (Figure 4a,c). This phenomenon was also seen in the force measurements discussed below. **Figure 5** shows an expanded plot of the angle of deflection measured at 5-second intervals during a single –3 V to +3 V actuation cycle, overlaid with the measured current. As discussed further below, from this plot it becomes apparent that the relaxation of the film during reduction occurs at a much slower rate than the expansion during oxidation. Thus, the expansion noted during the curing sequence could be attributed to a net accumulation of anions within the film, as the 1 Hz cycle rate does not allow sufficient time for complete expulsion of the ions. Alternatively, cation incorporation could be competing with anion expulsion, slowing the net contraction during reduction.[32,33]

When the cycling rate was slowed to two minute intervals to allow for complete reduction, the bilayers typically showed a ~10–20 degree angle of deflection, occasionally as high as 45 degrees. Larger movements were seen when the reduction time or voltage was increased, but this also resulted in more rapid degradation. For the studies shown here, a 3 V potential was used as a compromise between degradation and maximal

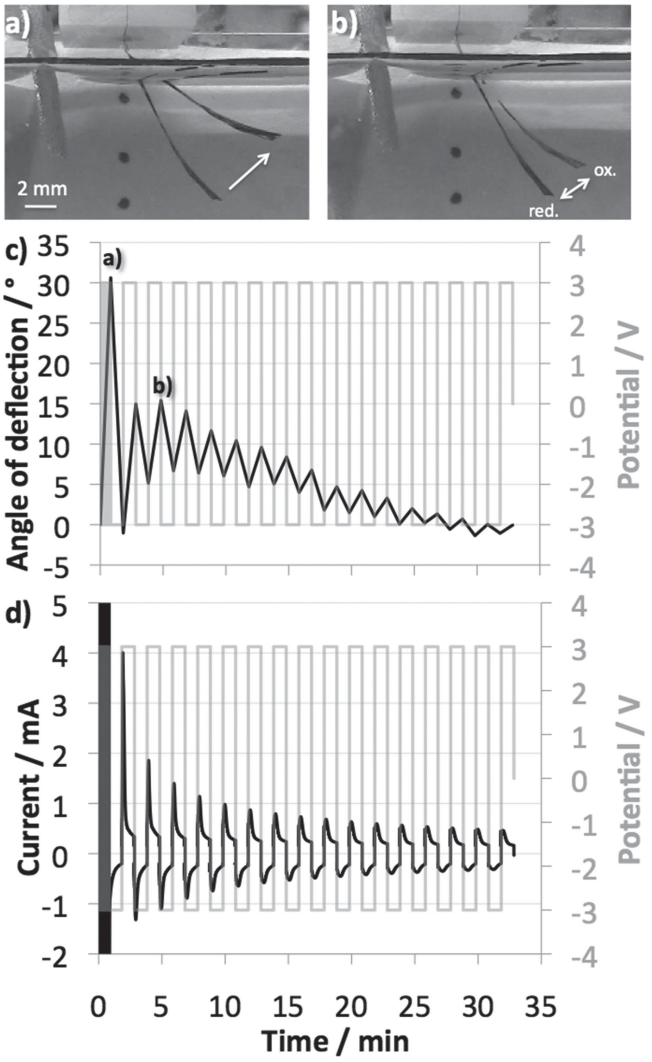

Figure 4. Representative free-end actuation behavior of a 3 × 10 mm silk-PPy film subjected to a ±3.0 V square wave for 50 cycles at 1 Hz, followed by 16 cycles at 1/120 Hz in PBS. Overlaid images are shown demonstrating macroscale movement a) during the curing sequence and b) during the second full actuation cycle. c) Plot of the applied voltage and the measured maximum angle of deflection relative to the initial position with each cycle. d) Current response measured over the entire experiment.

response. The current response spiked during each change in potential and rapidly decreased to a steady value after ~20 s (Figure 4d, Figure 5), indicating ion flow occurs predominantly when the potential is initially applied. The rate of bilayer movement also correlated with the current response,[23] which was greatest during the initial spike in current (Figure 5). During oxidation all movement occurs during the current spike in the first 20 s. However, more gradual change was noted during the reduction cycle. Film movement was greatest during the first 10 s, although the rate (slope) was less than half that seen during oxidation. After the first 10 s of reduction, the rate decreased and the film slowly continued to contract throughout the rest of the cycle. Similar behavior has been seen in other PPy actuators where anion transport prevails.[33,36] Possible

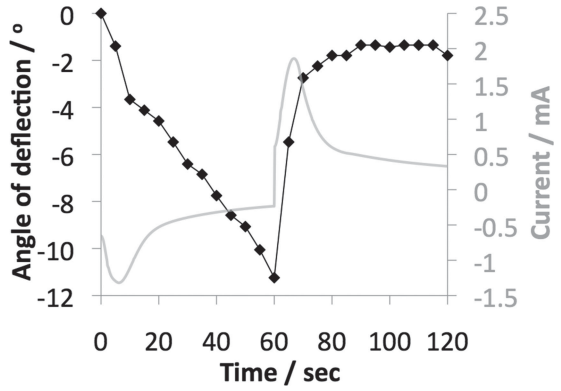

Figure 5. The angle of deflection measured at 5-second intervals during a single −3 V to +3 V actuation cycle (second full actuation from Figure 4), overlaid with the measured current. The initial angle was set at 0. The film is being reduced during the first 60 s, resulting in a negative angle due to contraction of the film.

explanations of the slow continued contraction at low current are expulsion of deeply-trapped ions, 'salt-draining' where neutral salts are slowly expelled from the polymer matrix, or reorganization of the polymer chains.[33,37]

4.2. Force Generation During Actuation

Further characterization of the forces generated during actuation was carried out using a tensile testing apparatus modified with a custom-built submersion chamber (see Supporting Information). A force transducer was installed in the upper fixture of the testing frame. The transducer was coupled to an inert plastic clamp containing a gold foil insert that clamped to the upper end of the films and made electrical contact. The other end of the film was clamped to the bottom of the submersion chamber mounted in the lower tensile fixture, which allowed the samples to be submerged in PBS during testing. A 2-electrode setup identical to the free-end bending actuation was used to apply potentials and read current changes.

Each sample was clamped, submerged and then ~0.2 N of force was applied to pull the films taut. Films were held in this pre-loaded state for 15 min to allow time for the polymer film to relax and attain a lower static stress, which helped to minimize drift due to creep during the actuation cycles.[42] After this period of relaxation, the silk-PPy films were subjected to the same conditions used for free-end actuation, ±3.0 V square wave for 50 cycles at 1 Hz, followed by 16 cycles at 1/120 Hz. **Figure 6** displays the change in stress of a sample over the entire experiment (initial relaxation omitted for clarity), and the currents measured during each cycle. Since the ends of the film are held, the values reported here only represent the linear component of the stress that is directed in the plane of the film. We are not taking into account the torque, or out of plane stresses. While the small stresses generated here approach the sensitivity limit of our instrumentation, we consistently observed an increase in stress during the oxidation phase of each actuation cycle, and a decrease in stress during the reduction phase. These observations correlate with behavior seen in the free-end bending, where the films expand during

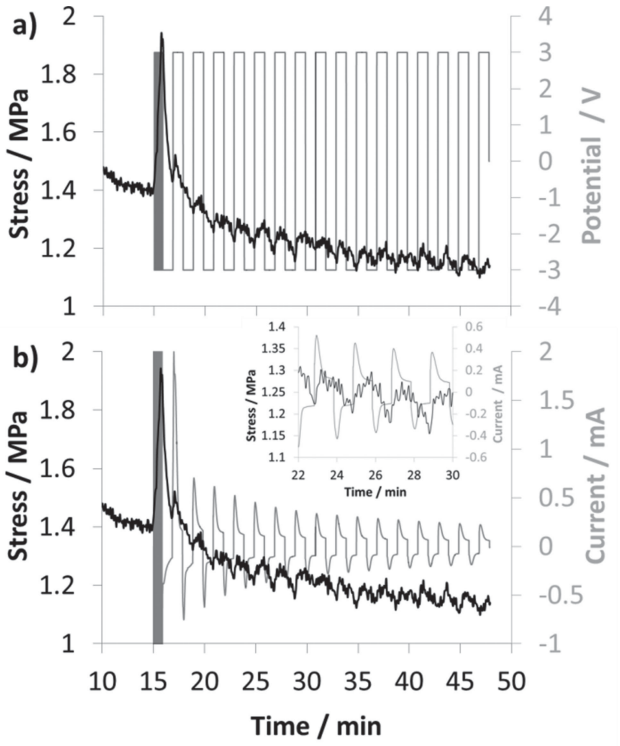

Figure 6. Representative plots showing a) the force generated and the b) current response measured during actuation of a silk-PPy film subjected to a ±3.0 V square wave for 50 cycles at 1 Hz, followed by 16 cycles at 1/120 Hz while submerged in PBS. The inset in (b) gives an expanded plot of several actuation cycles. The relaxation of the film during the first 10 minutes is omitted for clarity, but an initial load of 0.2 N (2.0 MPa) was applied to the film. The potential sequence was initiated at 15 min.

oxidation due to anion incorporation in the polymer matrix, which is seen here as a stiffening of the films. When anions are expelled from the matrix during reduction, the increase in free volume results in a relaxation of the polymer films leading to a decrease in stress.[33] While significant decay in movement was seen throughout free-end bending cycles, the magnitude of the force stayed fairly constant throughout the experiment, generating ~0.1 MPa (0.01 N) of stress upon each oxidation cycle.

As discussed above, a net expansion was observed during the curing sequence in the free-end bending actuators, where films moved twice as far as they did in subsequent cycles. Here, a corresponding phenomenon was noted, where a rise in stress associated with fast cycling reached magnitudes of >0.5 MPa (0.05 N), approximately 5 times larger than the subsequent actuation peaks. The current observed during fast cycling was also of a larger magnitude, reaching up to 15 mA.

During each oxidation and reduction phase, current spiked with the change in potential and then decayed to a non-zero value, but weak correlation between the magnitude of the current response and the magnitude of stress generated during actuation was noted. In the free-end actuations, the decreasing angle of deflection over time directly correlated to the decay in current response. Here, however, significantly higher forces were only generated during the curing sequence (15 mA), while the decay in current from 2 mA to 0.2 mA during the longer actuation cycles had little bearing on stress generated as both the first and last actuation exerted ~0.1 MPa. The lack of correlation could be due to lack of sensitivity in our instrumentation.

While these stress values are in the low range of that reported for CP-based actuators as discussed in the introduction,[9] the performance here was measured in a biologically-relevant environment, and did not use any organic solvents or electrolytes that would not be present *in vivo*. These silk-PPy composites compare favorably with human muscle that can generate between 0.1–0.5 MPa, making these materials ideal for interfacing with biological tissues. There is also substantial room for improvement of these first-generation devices through further optimization of the CP polymerization/deposition conditions, or through adjusting the processing parameters to control the mechanical properties and geometry of the silk support. The large spike in stress up to 0.5 MPa noted during the curing sequence suggests that further manipulation of the cycling parameters could also enhance performance.

5. Summary and Outlook

Here we demonstrate that films composed of an interpenetrating network of silk fibroin and PPy can function as electromechanical actuators in aqueous electrolytes. This is among the first demonstrations of a fully-biocompatible, metal-free actuator device operated in a biologically-relevant environment. The proof-of-concept experiments presented here with simple bilayer devices are currently being expanded to more complex device geometries. Silk can be processed into a variety of 3D forms including fibers, gels and porous network scaffolds, allowing facile extension of this work into 3D actuator device geometries that are not possible when using CPs alone. We are also pursuing methods to achieve better response at lower voltages through manipulation of the composite chemistry and microstructure. The redox sensitivity of these materials to different anions also presents intriguing possibilities for the use of these materials as biosensors or for electrochemical release of anionic drugs.

6. Experimental Section

Materials: All chemicals were purchased from Aldrich, Sigma or Fluka and used without further purification. Silk fibroin was obtained by harvesting cocoons produced by *Bombyx mori* silkworms reared in our laboratories, or from cocoons donated by the Tissue Engineering Resource Center (TERC) at Tufts University.

Instrumentation: Infrared spectra were measured on solid films in ambient atmosphere with a Fourier transform infrared (FTIR) spectrometer (ThermoScientific Nicolet IS10) equipped with an attenuated total reflectance (ATR) accessory. Topography of silk films were visualized by scanning electron microscopy (SEM) using a Vega TS 5136MM equipped with an energy dispersive X-ray (EDX) spectrometer. Films were mounted with carbon tape on aluminum stubs. Samples were conductive enough to be imaged directly, so no metal coating was used. Optical microscopy was performed using an Olympus SZX16 Optical Microscope. Sheet resistivity measurements were made with a Lucas Labs S-304–2 four-point resistivity probe (Signatone SP4–40045TBY tip) powered by a Keithley 2400 Source meter. Actuation experiments were also powered by a Keithley 2400 Source meter controlled by a LabView interface. Cyclic voltammetry experiments were carried out using a

Pine Research Instrumentation WaveNow potentiostat, and data was recorded and analyzed using AfterMath software. Counter and reference electrodes were purchased from Bioanalytical Systems, Inc.

Preparation of Aqueous Silk Solutions: Twelve cocoons from the *B. mori* silkworm were cut into pieces and rapidly boiled in an aqueous solution of 0.02 M Na_2CO_3 (3 L) for 1 h. The resulting fibers were rinsed once with boiling nanopure water, three times with room temperature water, and then dried at room temperature. The purified silk fibers were dissolved in a solution of 9 M LiBr at 60 °C for ~1 h to make a 20% (w/v) silk solution. This solution was placed into a dialysis cassette (Pierce Slide-a-lyzer G2, 3.5k MWCO, 5–15 mL capacity) or dialysis tubing (Fisherbrand, 3.5k MWCO, 6.74 mL/cm capacity), and dialyzed against 1 L nanopure water per dialysis cassette for three days, changing the water five times. The pH of the water was adjusted using HCl so that the final silk solution was pH 6–7. After removal, the resulting silk solution was filtered through a 5 μm pore size syringe filter. The final solution typically had a concentration of 7–8% (w/v), and was stored at 4 °C.

Preparation of Insoluble Silk Films: Silk solution prepared as described above was cast over a rectangular area of a silicone baking mat from a commercial retailer (1 mL silk solution per 12 cm^2 surface area), and allowed to air dry. Dried films were then removed from the silicone surface, and soaked in 70% ethanol overnight to render the films insoluble in water. The next day, the films were rinsed thoroughly with nanopure water and stored in water or dry. The visual difference between the side of the films dried touching the silicone surface and the side exposed to air was apparent, with the surface dried in contact with the silicone appearing dull compared to the side of the film dried in contact with the air.

Acid-Modification and PPy Deposition on Insoluble Silk Films: To create bilayer films, chemical modifications were made only to the porous, silicone-dried side of the silk films. Prior to each reaction, films were blotted dry and the edges were adhered to the bottom surface of Petri dishes with double-sided tape (3M Repositionable Tape, 666) to prevent reaction solution from leaking under the film. The porous silicone-dried surface faced up to the reaction solution. The diazonium reaction used to modify the top surface of the film with sulfonic acid groups and pyrrole polymerization reaction were carried out as previously described,[30] with slight modifications. Following acid-modification, films were rinsed thoroughly with nanopure water, and then exposed to an aqueous solution containing 50 mM pyrrole and 5 mM of sodium allyl sulfonate (AS) (used as the 'dopant'). To initiate polymerization, $FeCl_3$ (7.5 mM final concentration) was added and the solution was left to react for 1–2 h at room temperature. Films were cut out of the tape frame, rinsed thoroughly with nanopure water, and stored in water at room temperature.

Electrical Characterization: Sheet resistivity of the PPy-modified side of bilayer films was measured in ambient atmosphere with a Lucas Labs S-304–2 four-point resistivity probe (Signatone SP4–40045TBY tip) powered by a Keithley 2400 source meter. Sheet resistivity was calculated based on current-voltage relationships in the films using Equation (1)

$$R_s = 4.532 * (V/I), \quad (1)$$

where V (volts) is the voltage measured across the two inner electrodes, I (amperes) is the current passed between the two outer electrodes, and Rs (Ω/square) is the sheet resistivity. The actuator films had an average sheet resistivity of ~10^2 Ω/sq.

Cyclic Voltammetry: Cyclic voltammetry (CV) was carried out using a 3-electrode cell equipped with a platinum wire counter electrode, and an Ag/AgCl (in 3 M NaCl) reference electrode. Circular silk films (10–13 mm diameter) coated with PPy served as the working electrodes. Contact was made to the films using copper tape that was encapsulated in Kapton tape to allow the films to be completely submerged into the electrolyte. The area of films exposed to electrolyte was approximately 50 mm^2. Electrochemical studies were carried out in a range of aqueous supporting electrolyte solutions including phosphate buffered saline (PBS) (ThermoScientific BupH Phosphate Buffered Saline Packs, 0.1 M sodium phosphate, 0.15 M NaCl, pH 7.2) and 0.2 M solutions of NaCl, KCl, $CaCl_2$, $MgCl_2$, NaH_2PO_4, $NaHCO_3$, Na_2CO_3. Scans were initiated at 0 V and swept between ±1.0 V. For experiments looking at anion or cation sensitivity, a single film was initially cycled for 10 scans at a rate of 200 mV/s, then sequentially cycled in the buffers noted for 5 scans at a rate of 50 mV/s.

Actuation of Bilayer Films: Actuation experiments were carried using a 2-electrode system in PBS, utilizing the bilayer silk-PPy film as the working electrode and a 25 × 25 mm platinum mesh as the combined reference/counter electrode. Electrical contact was made to the films by mechanically fixing the end of the film to a gold foil using an inert plastic clamp. The clamp was then lowered so that the electrical contact was just above the solution interface. Actuator films (3 mm × 10 mm × 0.05 mm) were positioned with the PPy-modified side facing the platinum electrode. Prior to actuation, films were initially subjected to a 'curing cycle,' in which a square wave (±3.0 V) was applied to the sample for 50 cycles at 1 Hz using a Keithley Source meter 2400 controlled by LabView. Immediately following this curing cycle, films were actuated by applying a square wave (±3.0 V) at 1/120 Hz for the specified number of cycles. Video recordings were made of each actuation, and the maximum angle of deflection was measured on overlaid still-frame images using ImageJ. Rates of movement were calculated based on frame-by-frame analysis of the actuation videos.

Force Generation During Actuation: To measure the forces generated during actuation, the conditions outlined for actuation experiments above were replicated while the films were held in a retrofitted tensile testing frame. In the upper fixture of an MTS Sintech frame, a 25 lbf capacity force transducer (MTS #100–090–900) was installed. The transducer was connected to an inert plastic clamp containing a gold foil insert, which served to clamp the upper end of the films and make electrical contact. The other end of the films were held by a rubber-faced clamp in the bottom of a custom-built submersion chamber mounted in the lower fixture of the MTS, which allowed the samples to be submerged in PBS during testing. A small load (~0.2 N) was applied to the actuator films (3 mm × 10 mm × 0.05 mm) for 15 minutes to pull the films taut and minimize drift during the actuation cycles due to creep. Curing and actuation cycles were carried out as described above. TestWorks® 4 software was used to operate the MTS Sintech frame and record the force generated, while a separate computer executed the curing and actuation cycles in LabView as described above. Force measured in N was divided by the cross-sectional area of the films to arrive at the stress reported in MPa.

Supporting Information

Supporting Information is available from the Wiley Online Library or from the author.

Acknowledgements

We are grateful for financial support from Western Washington University, a grant to WWU's Advanced Materials Science and Engineering Center (AMSEC) from the M.J. Murdock Charitable Trust, the donors of the American Chemical Society Petroleum Research Fund (AM), and the National Science Foundation (CAREER DMR-1057209) (JL). We thank David Kaplan and the Tissue Engineering Resource Center (TERC) at Tufts University for providing silk cocoons. We thank Erin Macri and Charles Wandler in Scientific and Technical Services at WWU for assistance with SEM, and Prof. Nicole Larson in Engineering Technology for help with mechanical testing. We also thank Alex Streck for designing the first prototype submersion chamber.

Received: September 23, 2013
Revised: January 30, 2014
Published online: March 20, 2014

[1] E. Smela, *Adv. Mater.* **2003**, *15*, 481.
[2] T. Shoa, J. D. Madden, N. R. Munce, V. Yang, *Polym. Int.* **2010**, *59*, 343.
[3] H. Tsai, M. Madou, *J. Lab. Autom.* **2007**, *12*, 291.
[4] R. H. Baughman, *Synth. Met.* **1996**, *78*, 339.
[5] M. Asplund, T. Nyberg, O. Inganäs, *Polym. Chem.* **2010**, *1*, 1374.
[6] R. A. Green, N. H. Lovell, G. G. Wallace, L. A. Poole-Warren, *Biomaterials* **2008**, *29*, 3393.
[7] G. M. Spinks, V. Mottaghitalab, M. Bahrami-Samani, P. G. Whitten, G. G. Wallace, *Adv. Mater.* **2006**, *18*, 637.
[8] S. Hara, T. Zama, W. Takashima, K. Kaneto, *Polym. J.* **2004**, *36*, 933.
[9] F. Carpi, E. Smela, Biomedical Applications of Electroactive Polymer Actuators, John Wiley & Sons, USA **2009**.
[10] A. S. Hutchison, T. W. Lewis, S. E. Moulton, G. M. Spinks, G. G. Wallace, *Synth. Met.* **2000**, *113*, 121.
[11] M. Pyo, C. C. Bohn, E. Smela, J. R. Reynolds, A. B. Brennan, *Chem. Mater.* **2003**, *15*, 916.
[12] E. Smela, O. Inganäs, I. Lundström, *Science* **1995**, *268*, 1735.
[13] B. Gaihre, G. Alici, G. M. Spinks, J. M. Cairney, *Sens. Actuat. B* **2011**, *155*, 810.
[14] R. Temmer, I. Must, F. Kaasik, A. Aabloo, T. Tamm, *Sens. Actuat. B* **2012**, *166*, 411.
[15] K. Ikushima, S. John, A. Ono, S. Nagamitsu, *Synth. Met.* **2010**, *160*, 1877.
[16] A. Khaldi, C. Plesse, C. Soyer, E. Cattan, F. Vidal, C. Legrand, D. Teyssié, *Appl. Phys. Lett.* **2011**, *98*, 164101.
[17] F. Vidal, C. Plesse, G. Palaprat, A. Kheddar, J. Citerin, D. Teyssié, C. Chevrot, *Synth. Met.* **2006**, *156*, 1299.
[18] F. Vidal, C. Plesse, P.-H. Aubert, L. Beouch, F. Tran-Van, G. Palaprat, P. Verge, P. Yammine, J. Citerin, A. Kheddar, L. Sauques, C. Chevrot, D. Teyssié, *Polym. Int.* **2010**, *59*, 313.
[19] F. Vidal, J. F. Popp, C. Plesse, C. Chevrot, D. Teyssié, *J. Appl. Polym. Sci.* **2003**, *90*, 3569.
[20] C. Plesse, F. Vidal, D. Teyssié, C. Chevrot, *Chem. Commun.* **2010**, *46*, 2910.
[21] H.-J. Choi, Y.-M. Song, I. Chung, K.-S. Ryu, N.-J. Jo, *Smart Mater. Struct.* **2009**, *18*, 024006.
[22] F. García-Córdova, L. Valero, Y. A. Ismail, T. F. Otero, *J. Mater. Chem.* **2011**, *21*, 17265.
[23] L. Valero, J. Arias-Pardilla, J. Cauich-Rodríguez, M. A. Smit, T. F. Otero, *Electrochim. Acta* **2011**, *56*, 3721.
[24] G. M. Spinks, S. R. Shin, G. G. Wallace, P. G. Whitten, I. Y. Kim, S. I. Kim, S. J. Kim, *Sens. Actuat. B* **2007**, *121*, 616.
[25] Y. A. Ismail, S. R. Shin, K. M. Shin, S. G. Yoon, K. Shon, S. I. Kim, S. J. Kim, *Sens. Actuat. B* **2008**, *129*, 834.
[26] Y. A. Ismail, J. G. Martinez, A. S. Al Harrasi, S. J. Kim, T. F. Otero, *Sens. Actuat. B* **2011**, *160*, 1180.
[27] G. H. Altman, F. Diaz, C. Jakuba, T. Calabro, R. L. Horan, J. Chen, H. Lu, J. Richmond, D. L. Kaplan, *Biomaterials* **2003**, *24*, 401.
[28] Y. Wang, H.-J. Kim, G. Vunjak-Novakovic, D. L. Kaplan, *Biomaterials* **2006**, *27*, 6064.
[29] A. R. Murphy, P. St. John, D. L. Kaplan, *Biomaterials* **2008**, *29*, 2829.
[30] I. S. Romero, M. L. Schurr, J. V. Lally, M. Z. Kotlik, A. R. Murphy, *ACS Appl. Mater. Interfaces* **2013**, *5*, 553.
[31] P. G. A. Madden, J. D. W. Madden, P. A. Anquetil, N. A. Vandesteeg, I. W. Hunter, *IEEE J. Oceanic Eng.* **2004**, *29*, 696.
[32] R. Ansari Khalkhali, W. E. Price, G. G. Wallace, *React. Funct. Polym.* **2003**, *56*, 141.
[33] Q. Pei, O. Inganäs, *Solid State Ionics* **1993**, *60*, 161.
[34] J. Yang, D. C. Martin, *Sens. Actuat. A* **2004**, *113*, 204.
[35] H. Yamato, M. Ohwa, W. Wernet, *J. Electroanal. Chem.* **1995**, *397*, 163.
[36] R. John, G. G. Wallace, *J. Electroanal. Chem.* **1993**, *354*, 145.
[37] J. Tanguy, N. Mermilliod, *Synth. Met.* **1987**, *21*, 129.
[38] H. Yang, J. Kwak, *J. Phys. Chem. B* **1997**, *101*, 774.
[39] W. Takashima, S. S. Pandey, K. Kaneto, *Sens. Actuat. B* **2003**, *89*, 48.
[40] A. Della Santa, D. De Rossi, A. Mazzoldi, *Smart Mater. Struct.* **1997**, *6*, 23.
[41] J. D. Madden, R. A. Cush, T. S. Kanigan, I. W. Hunter, *Synth. Met.* **2000**, *113*, 185.
[42] J. D. Madden, D. Rinderknecht, P. A. Anquetil, I. W. Hunter, *Sens. Actuat. A* **2007**, *133*, 210.